This is the Post-print version of the following article: ***E. Toral-Sánchez, Juan A. Ascacio Valdés, Cristóbal N. Aguilar, F.J. Cervantes, J.R. Rangel-Mendez, Role of the intrinsic properties of partially reduced graphene oxides on the chemical transformation of iopromide, Carbon, Volume 99, 2016, Pages 456-465,*** **which has been published in final form at: https://doi.org/10.1016/j.carbon.2015.12.067**

© 2016. This manuscript version is made available under the Creative Commons Attribution-NonCommercial-NoDerivatives 4.0 International (CC BY-NC-ND 4.0) license http://creativecommons.org/licenses/by-nc-nd/4.0/

Accepted Manuscript

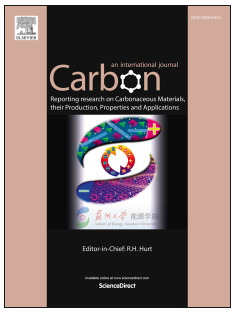

Role of the intrinsic properties of partially reduced graphene oxides on the chemical transformation of iopromide

E. Toral-Sánchez, Juan A. Ascacio Valdés, Cristóbal N. Aguilar, F.J. Cervantes, J.R. Rangel-Méndez

PII: S0008-6223(15)30533-9

DOI: 10.1016/j.carbon.2015.12.067

Reference: CARBON 10593

To appear in: *Carbon*

Received Date: 14 September 2015

Revised Date: 16 December 2015

Accepted Date: 18 December 2015

Please cite this article as: E. Toral-Sánchez, J.A. Ascacio Valdés, C.N. Aguilar, F.J. Cervantes, J.R. Rangel-Méndez, Role of the intrinsic properties of partially reduced graphene oxides on the chemical transformation of iopromide, *Carbon* (2016), doi: 10.1016/j.carbon.2015.12.067.

This is a PDF file of an unedited manuscript that has been accepted for publication. As a service to our customers we are providing this early version of the manuscript. The manuscript will undergo copyediting, typesetting, and review of the resulting proof before it is published in its final form. Please note that during the production process errors may be discovered which could affect the content, and all legal disclaimers that apply to the journal pertain.

ACCEPTED MANUSCRIPT

Role of the intrinsic properties of partially reduced graphene oxides on the chemical transformation of iopromide

E. Toral-Sánchez[1], Juan A. Ascacio Valdés[2], Cristóbal N. Aguilar[2], F.J. Cervantes[1],J.R. Rangel-Méndez[1]*

[1]División de Ciencias Ambientales, Instituto Potosino de Investigación Científica y Tecnológica A.C. Camino a la Presa San José 2055, Col. Lomas 4a. Sección, C.P. 78216, San Luis Potosí, SLP, México

[2]Facultad de Ciencias Químicas. Departamento de Investigación en Alimentos (DIA-UAdeC), Universidad Autónoma de Coahuila. Saltillo, 25280, Coahuila, México.

*Corresponding author. E-mail address: rene@ipicyt.edu.mx (J.R. Rangel-Méndez) Fax: +52 444 834 2010

Abstract

The role of the intrinsic properties of graphene oxide (GO) and partially reduced graphene oxide (rGO), and their use as redox mediator (RM) is reported, for the first time, on the chemical transformation of iopromide (IOP), an iodinated X-ray contrast medium, under anaerobic conditions. The structural and physicochemical properties of GO containing different types of oxygenated groups, were analyzed by Boehm titrations, point of zero charge (pH_{PZC}), pKa's distribution, scanning electron microscopy (SEM), electrochemical analysis, as well as by Raman, Fourier transform infrared and UV-Vis spectroscopy. Complete characterization of GO-based materials revealed the removal of different oxygenated groups, such as epoxy and hydroxyl groups, and a transition from an amorphous to a more crystalline structure on partially reduced GO. Moreover, when rGO materials were tested as RM, they promoted a faster and greater extent of IOP transformation up to 5.2-fold with sulfide as electron donor. Results showed a correlation between the reduction degree of GO and its ability to act as RM, which was reflected in the dehalogenation and transformation degree of IOP. Additionally, the chemical transformation pathway of IOP is proposed based on HPLC-MS analysis.

1. Introduction

Graphene is a two-dimensional crystal structure with a thickness of one atom, and is composed of sp^2-bonded carbon atoms densely packed in two crystal sub-networks [1]. Such two-dimensional carbon sheet possesses unique properties such as, mechanical strength, high surface area (2600 m^2/g [2]) and rapid electron transfer capacity [3], which promote its broad application in sensors, nanoelectronics, biomedicine, capacitors, among other industrial uses [1]. Also, graphene-based nanomaterials possess distinct open edges around their periphery, allowing to have high reactivity due to their nonbonding π-electrons [4] and therefore, extraordinary catalytic activities are observed [5,6]. In addition, graphene-based materials, such as graphene oxide (GO), present a wide array of oxygenated groups in their chemical structure like hydroxyl, epoxy, carboxyl and carbonyl groups [7]. In this sense, it has been reported that the use of chemical substances with quinone groups (two carbonyl groups [8]) in their structure can mediate the transformation of recalcitrant pollutants by enhancing electron transfer processes [9–11]. Such chemical substances with the capacity to receive and yield electrons are known as redox mediators (RM) and they have been applied to accelerate the transformation of recalcitrant pollutants [12]. On the other hand, it was reported that the graphene basal planes of GO-based materials have very high electric conductivity [13,14], which has been reported as another mechanism to mediate the reductive transformation of recalcitrant pollutants by enhancing electron transfer, due to the electric conductivity properties of the graphitic carbon surface [5].

Carbon materials like activated carbon, activated carbon fibers, carbon xerogel, graphite and carbon nanotubes (CNT), have been used as RM in the reductive transformation of recalcitrant pollutants such as azo dyes [9,11,15], nitroaromatic compounds[16–21], nitramine compounds [17,22–24], nitroglycerin [25], nitro herbicides [26], dibromophenol [27], and tetrachloroethane [28], since they have a diversity of surface oxygenated groups like quinone groups, which can mediate the reduction of these pollutants. Recently, it was shown that graphene-based materials, such as GO and reduced graphene oxide (rGO), can facilitate the reduction of some recalcitrant pollutants by enhancing electron transfer [9,29]. For example, Colunga et al., [30] reported the use of GO as RM for the biotic and abiotic

reduction of an azo dye (reactive red 2) and 3-chloronitrobenzene, showing that the presence of GO increased up to 10-fold and 3.6-fold the abiotic and biotic reduction, respectively. Similarly, Lu et al., [31] reported a removal up to 90% for biotic and abiotic reduction of acid yellow 36 using a quinone-rGO composite as RM. Fu and Zhu [5] and Gao et al., [6] evaluated the abiotic reduction of nitrobenzene using GO and rGO as RM, respectively, concluding that the properties of these carbon materials facilitated the reduction of this pollutant. Also, Wang et al., [32] reported an increase up to 2-fold in the biotic transformation of nitrobenzene when a rGO-anaerobic sludge composite was used as novel biocatalyst. Fu et al., [33] tested the capability of GO and CNT on the reductive dechlorination of hexachloroethane, concluding that the mediation efficiency of these materials is 10 times higher than humic acid material. Finally, Oh et al., [21] investigated the abiotic reduction of nitroaromatic compounds, such as dinitrotoluene, pendimethalin and trifluralin using rGO and CNT as RM, achieving a removal for the tree pollutants of around 50% and 88% for CNT and rGO, respectively. Therefore, it can be inferred that graphene-based materials could mediate redox reactions involved in the transformation of recalcitrant pollutants. However, the use of these nanomaterials on the abiotic transformation of pharmaceutical compounds has not been reported yet.

Iodinated X-ray contrast media (ICM), such as iopromide (IOP), are pharmaceuticals widely used in intravascular administration with a global consumption of approximately 3.5 x 10^6 Kg per year [34]. IOP is a priority pollutant, which is beginning to be studied because of its high recalcitrance through conventional wastewater treatment, as well as in environment compartments. Moreover, IOP has been detected in effluents from sewage treatment plants, surface water systems, groundwater, and even in drinking water at μg/L levels [35,36]. In addition, it has been reported that 15 % of people who have been exposed to this pharmaceutical have suffered some adverse reactions such as nauseas, vomiting, headache, hives, etc. [37]. Recent reports indicate that IOP is poorly removed in conventional wastewater treatment facilities and thus it is released into receiving water bodies [38–40]. Its recalcitrance is attributed to low biodegradability by aerobic bacteria [41] and to the high hydrophilicity of the benzene ring substituents (hydroxyl and carboxyl groups) [36]. As a consequence, it is necessary to propose strategies for the reductive transformation of this recalcitrant pollutant.

The aim of the present work was to evaluate the intrinsic properties of both GO and partially reduced GO and their effect on the abiotic transformation of IOP in basal medium, conducted in batch systems, and to explain the reduction mechanisms taking place under non-oxidizing conditions. Additionally, the chemical surface and morphological characterization was carried out by Fourier transform infrared spectroscopy, Boehm titrations, point of zero charge (pH_{PZC}), pKa's distribution, scanning electron microscopy (SEM), electrochemical analysis, Raman and UV-Vis spectroscopy, in order to elucidate the importance of these properties in the ability to act as electron shuttle.

2. Experimental

2.1. Chemicals

All chemicals with 99% purity were used as received. IOP (CAS No. 73334-07-3) was obtained from Bayer Schering Pharma (Mexico City, Mexico) with commercial name Ultravist® 370; L-ascorbic acid (L-AA, ACS grade) from GOLDEN BELL (Mexico City, Mexico) and sodium sulfide ($Na_2S \cdot 9H_2O$) from Fisher-Scientific (New Jersey, USA). The basal medium (pH = 7.6) used in abiotic reduction assays was composed of (g/L): K_2HPO_4 (0.25), $NaHCO_3$ (5.0), $MgSO_4 \cdot 7H_2O$ (0.1), NH_4Cl (0.28), $CaCl_2 \cdot 2H_2O$ (0.01), and trace elements (1 mL/L), with a composition described elsewhere [10]. A phosphate buffer (pH= 7.0) was used during electrochemical analysis with a composition of (g/L): K_2HPO_4 (3.32) and KH_2PO_4 (4.21). All chemicals used for basal medium and phosphate buffer elaboration were obtained from either Sigma-Aldrich or Merck. All solutions were prepared with deionized water (18.1 MΩ·cm).

Graphene oxide used in the present study was purchased from Graphene Supermarket® (New York, USA), with the following characteristics: high density and viscosity, concentration of 6.2 g/L in aqueous solution, single-layer > 60 %, flake size between 0.5 and 5 µm, C/O ratio 3.95.

2.2. Chemical reduction of GO

GO was reduced with L-AA as follows: 10 mL of GO solutions (0.1 mg/mL) and 100 mg of L-AA were placed in a 30 mL beaker. Immediately, samples were vigorously stirred at room temperature. In order to obtain materials with different reduction degrees, reduction

kinetics of GO were carried out for 0.5, 1, 1.5, 2, 3 and 4 hours. After the reduction time, samples were centrifuged at 13,300 rpm for 10 min in order to remove all L-AA remaining by decantation. Recovered rGO was rinsed with deionized water three times and then dispersed in the same medium (deionized water).

2.3. Physical and chemical characterization of GO-based materials

2.3.1. Zeta potential and oxidation reduction potential (ORP)

Zeta potential measurements of samples were performed in aqueous solution at pH 7.0 in a MICROTRAC Zetatrac NPA152-31A equipment. On the other hand, ORP of GO samples and of IOP were assessed under experimental conditions of chemical reduction using a Thermo Scientific electrode with a reference solution of Ag/AgCl Orion 900011 (+415 mV at 30°C). All ORP measurements were performed inside an anaerobic chamber with a N_2:H_2 (95:5% v/v) atmosphere.

2.3.2. Chemical characterization of GO samples

Fourier transform-infrared (FT-IR) spectra were recorded on a Thermo-Scientific FTIR (Nicolet 6700 model) spectrophotometer in transmission mode with a resolution of 4 cm^{-1} and 128 scans. For sample preparation, GO-based materials were mixed with KBr at a ratio of 1:99% (w/w) for subsequent drying at 60 °C for 48 h, and then compressed into a transparent pellet for measurement.

Carbonyl, phenolic, lactonic and carboxylic groups were quantified by potentiometric titrations as described by Boehm [42] with an automatic titrator (Mettler-Toledo T70) as follow: 0.05 g/L of GO-based materials were contacted with 25 mL of neutralizing solutions. The solutions were continuously stirred at 125 rpm for 5 days. After that, samples were titrated with 0.1 N HCl. The point of zero charge (pH_{PZC}) of GO-based materials was determined according to Bandosz [43] with the automatic titrator mentioned above. For this procedure, 0.005 mg/mL of GO-based materials were contacted with 25 mL of 0.01 N NaCl. The solutions were stirred at 125 rpm for 24 h. Finally, the samples were titrated with 0.1 N NaOH. The surface charge and pKa distributions were determined by the SAEIU-pK-Dist© (1994) program [44].

147 2.3.3. Morphological and optical properties

148 Microscopic observations were carried out on a FEI Helios Nanolab 600 Dual Beam
149 Scanning Electron Microscope (SEM) operated at 5.00 kV and 86 pA. Samples were
150 suspended in isopropanol and then sonicated for 30 min. Elemental analyses were carried
151 out by energy dispersive spectrometer (EDS) on the same equipment. Raman spectra were
152 recorded at room temperature with a RENISHAW Micro-Raman Invia spectrometer with
153 laser frequency of 514 nm as excitation source trough a 50 X objective. UV-Vis
154 transmittance spectra of GO-based materials in aqueous dispersion were collected by a
155 Thermo Spectronic Aqua Mate UV-Vis spectrophotometer at a wavelength of 550 nm. The
156 wavelength scan was performed from 400 to 600 nm using deionized water as blank.

157 2.3.4. Electrochemical characterization

158 Electrochemical analysis of GO-based materials was assessed by cyclic voltammetry (CV)
159 technique using a VSP SAS Biologic system controlled by the EC-Lab software V 10.23
160 with a three-electrode cell configuration containing a Ag/AgCl/KCl (sat) as the reference
161 electrode, and a graphite rod and glassy carbon electrode (GCE) as the counter and working
162 electrode, respectively. The electrolytic solution was a phosphate buffer at pH 7.0 (See
163 section 2.1) saturated with argon for 5 min. All experiments were carried out at room
164 temperature. The working electrode was prepared as follows, GO or rGO was dispersed in
165 ethanol (spectrophotometric grade) and then 8 µL were suspended in the GCE surface.
166 Ethanol was volatilized and the material remained deposited on the GCE surface. Before
167 deposition, the GCE was polished in a nylon cloth with alumina suspension.

168 2.4.Adsorption isotherms

169 These experiments were conducted to evaluate the IOP adsorption capacity of the GO-
170 based materials at pH of basal medium (pH= 7.6, see Section 2.1). Into plastic tubes of 15
171 mL of capacity, 5 mg/L of materials and IOP (from 200 to 800 µg/L) were added.
172 Afterwards, the tubes were filled with basal medium to give a total volume of 10 mL.
173 Samples were kept under stirring and constant temperature (125 rpm and 25 °C) for 5 days.
174 The remaining concentration of IOP in solution was measured by high-performance liquid
175 chromatography (HPLC) as described in Section 2.6.

176 2.5. Chemical transformation of iopromide

177 The capacity of GO-based materials to serve as RM in the chemical transformation of IOP
178 was evaluated providing Na_2S as primary electron donor. Sulfide is an important reducing
179 compound commonly found in several industrial effluents, and their use as electron donor
180 for redox conversion of different pollutants has been reported [12]. To assess this abiotic
181 reduction, batch incubations were prepared in 60 mL serum flasks as follow: 5 mg/L of GO
182 or rGO were contacted with basal medium and then bubbled for 5 min with a gas mixture
183 of N_2:CO_2 (80:20 %). The flasks were sealed and the gas headspace was flushed for 3 min
184 with the gas mixture mentioned above. Inside an anaerobic chamber (N_2:H_2 (95:5%)
185 atmosphere), sulfide was added from a Na_2S stock solution to obtain a final concentration
186 of 2.6 mM. Bottles were incubated for 24 h with constant stirring and temperature (125 rpm
187 and 25 °C). After pre-incubation, IOP was added from an anaerobic stock solution in order
188 to obtain an initial concentration of 400 µg/L. The total working volume was 50 mL in all
189 incubations. The experiments were carried out for 13 days in the dark. Samples of 1 mL
190 were taken at selected times and the concentration of IOP was measured as described in
191 Section 2.6. Control experiments without GO-based materials and/or Na_2S were performed
192 to evaluate the stability of IOP, the direct reduction by sulfide and the adsorption onto the
193 materials.

194 2.6. Analytical procedures

195 The concentration of IOP was measured by HPLC using a Agilent Technology 1260 series
196 chromatograph, equipped with a column synergi 4U Hydro-RP 80R (250 x 4.60 mm, 4
197 micron) from Phenomenex. Forty microliters of sample were injected with an autosampler.
198 The mobile phase, composed of HPLC grade water and acetonitrile (85:15 %), was pumped
199 at a flow rate of 0.5 mL/min. IOP was detected at 30 °C and wavelengths of 238 nm with
200 an Agilent Technologies diode array detector. For the quantification of IOP concentration
201 in solution during adsorption and chemical reduction experiments, a calibration line with
202 different concentrations of IOP (from 100 to 1000 µg/L) in basal medium was performed.
203 The peak area according to each concentration was measured in a retention time of 11.6
204 min. The detection limit was 100 µg/L.

The transformation products of IOP were identified by HPLC coupled to mass spectroscopy (HPLC-MS) in a Varian ® 500-MS ion trap mass spectrometer, with electrospray ionization of 90 V and mass-to-charge (m/z) range of 100 to 2000 m/z.

3. Results and discussion

3.1.Characterization of GO and rGO materials

Seven samples of GO-based materials with different reduction degrees were analyzed by zeta potential and ORP. As known, zeta potential is a physical property exhibited by any material in dispersion and measures the potential difference between the dispersion medium and the stationary layer of fluid attached to dispersed particles [45,46]. Fig. 1 shows that zeta potential values increased from -23.41 to 25.26 mV as GO (unreduced GO, urGO) was farther reduced for up to 4 h (rGO-4). Negative zeta potential values are due to the presence of negatively charged functional groups, like oxygenated groups, present at the graphitic layers [47]. When the reduction degree of GO increased, a greater concentration of negatively charged functional groups are eliminated in GO sheets, resulting in an increase on zeta potential values [46]. For this reason, rGO-4 has the most positive zeta potential value (25.26 mV).

ORP is an important parameter to assess the ability of a chemical compound to accept or donate electrons under particular conditions [48]; therefore, it is a fundamental parameter related to the redox mediating activity. In this sense, carbon materials, like GO, exhibit redox activity, which is related to the oxygenated functional groups in the material [49]. The results reported also in Fig. 1 show that ORP noticeably increased from 60.8 mV for urGO to 501.9 mV for rGO-4 as GO was less oxidized, which may be because aromatic ring substituents, such as carbonyl groups, tend to accept electrons when oxygenated groups are eliminated from the basal plane [8,50,51]. Also, it has been reported that quinone groups (a couple of carbonyl groups) can act as electron acceptors [8]. In this sense, the electron activity of quinone groups consist in that carbonyl groups can act in concert to stabilize radicals via resonance. Resonance considerations permit the stabilization of radicals in equilibrium with quinonoid structures. After that, these radicals can accept electrons and become anions. Next, the anions can transfer electrons back and become radicals, or they can interact with protons in solution. Finally, the reversible proton

transfer leads to form of phenolic (hydroquinone) sites [8]. As will be discussed below, the carbonyl groups remain after reduction of GO, which might satisfactorily explain the increase in ORP values due to their ability to accept electrons as explained above.

According to these results, three samples were selected for further analysis: urGO, rGO for 2 h (rGO-2) and rGO-4 since they contain a low, intermediate and high ORP, which should be a key factor on the electrons transfer during the chemical reduction of IOP.

Photographic images of urGO, rGO-2 and rGO-4 are shown in supplementary material (SM, Fig. 1S). A color change from brownish yellow (Fig. 1S-a) to black (Fig. 1S-c) was observed as the reduction degree of urGO was greater, which is probably a result of an increase in the hydrophobicity of rGO materials, caused by the removal of oxygenated groups, that subsequently causes the agglomeration of graphene-based nanosheets [13] as can be seen in the micrographs reported in SM (Fig. 2S).

Several studies have reported that transmittance spectra can be used to determine the transparency of GO, which is intrinsically linked to its morphology [52,53]. Nair et al., [54] estimated that each graphene sheet reduces 2.3 % the transmittance at 550 nm. Therefore, the number of sheets in GO samples was measured under these experimental conditions. Transmittance percent at 550 nm was obtained from the corresponding spectra and it is shown in SM (Fig. 3S). Insert of Fig. 3S, depicts the estimated number of sheets in each sample in aqueous suspension according to Nair et al. [54]. It can be observed that the sheets number integrating the GO-based materials is approximately 6, 22 and 27 for urGO, rGO-2 and rGO-4, respectively. This can be attributed to the removal of oxygenated groups as a result of the chemical reduction, which consequently produces hydrophobic graphene sheets that tend to restack due to strong π-π interactions [55]. Hence, graphitic layers are attached to each other, forming materials consisting of a greater number of sheets.

Raman spectroscopy was employed to distinguish the ordered and disordered crystal structures of GO-based materials. Fig. 2 shows Raman spectra of urGO and rGO samples. The presence of G and D bands for urGO spectrum at 1599 cm^{-1} and 1354 cm^{-1}, respectively, is evident. The D band corresponds to defects in the graphite network, which are related to the presence of edges of graphitic planes, atomic vacancies, bond-angle

disorders, bond-length disorders or oxygenated groups [56,57]. On the other hand, the G band is related to defect-free graphite networks [58], corresponding to the first-order scattering of E2g mode [59]. The reduction of GO should result in structural changes, therefore, it is expected that GO undergoes morphological changes after it has been chemically reduced due to the removal of different oxygenated groups at the basal plane and also at the edges. Raman spectra for rGO-2 and rGO-4 confirm this observation (see Fig. 2). The G band is moved to a lower wavelength (1595 cm^{-1}), which is closer to the reported value for pristine graphite (1570 cm^{-1}), indicating that the chemical reduction of GO was conducted [60]. Moreover, the relative intensity of the D band around 1350 cm^{-1} increases as the reduction degree is higher, which apparently contradicts the idea that the reduction process should restore the graphitic order as expected by theory. This behavior can be explained due to the holes formed by CO and CO_2 evolution from oxygenated groups removal forming internal edge sites, which might increase the D band upon deoxygenation. On the other hand, Stankovich et al., [13] suggested that this behavior is due to that reduction increases the number of aromatic domains of smaller overall size in graphene, which would lead to an increase of the I_D/I_G ratio as will be discussed later. However, Paredes et al., [61] are at odds with this assumption based on the decrease of the 2D band at 2920 cm^{-1} of GO spectrum. They suggest that this contradiction can be explained by assuming that the carbon lattice in GO has certain degree of amorphous character due to the oxidation process itself [61]. Because the GO sheets contain many oxygenated groups in their chemical structure, a significant distortion of the aromatic rings occurs, and hence, a certain amorphous character is expected after the reduction process due to the remaining oxygenated groups in this material [62]. Therefore, an increase in the intensity of the D band after the GO chemical reduction can be possible [13] as reported by several studies [13,60–63].

On the other hand, it can be seen that the intensity ratio I_D/I_G increased with the reduction degree as follows: 0.56, 0.88 and 1.16 for urGO, rGO-2 and rGO-4, respectively. This change suggests a decrease in the average size of the sp^2 domains after chemical reduction of GO [59], due to the partially ordered graphite crystal structure of graphene sheets [13]. Many equations have been employed to estimate the average crystallite size of the sp^2 domains (La) in GO samples using the I_D/I_G ratio [59,64]. Hence, the La values (in nm) of

the GO-based materials under study were calculated based on the Cancodo et al., modified equation [65]. The calculated La values are 29.99, 19.48 and 14.69 nm for urGO, rGO-2 and rGO-4, respectively. These results indicate that the average crystallite size decreased as the reduction degree of the samples is higher, which can be due to the breakdown of crystallites with initial oxidation [46]. Also, this decrease can be explained by the creation of new graphitic sp^2 domains, which are smaller in size than those present in urGO [13]. The La values showed the transition from amorphous GO to a more crystalline form as the reduction grade advanced.

It is clear that the surface chemical properties of GO changed as it was reduced, as shown in Table 1. The total concentration of acidic groups decreased from 4.39 to 1.65 milli-equivalents (meq)/g when GO was chemically reduced for 4 h, mainly due to the removal of carboxylic, lactonic and phenolic groups. Moreover, we can observe a reduction percentage (based on total concentration of oxygenated groups) of 19.1 and 64.4 for rGO-2 and rGO-4, respectively. Also, a slight decrease on carbonyl groups was observed, from 1.23 to 1.1 meq/g. Chemical deoxygenation of GO is complex and may be selective to certain groups, depending on the reducing reagent. In this sense, the binding energy between graphene sheets and different oxygenated groups can be an important index to evaluate the reduction of each group attached to the carbon plane [66]. Kim et al., [67] reported that epoxy groups are more stable than hydroxyl groups in GO. However, Gao et al., [68] reported that oxygenated groups attached to the inner aromatic domain are not stable at room temperature and hence, they are removed more easily than those attached at the edges of an aromatic domains. In addition, the authors suggested, based on theoretical calculations, that carboxylic groups are slowly reduced, while carbonyl groups are much more stable. As can be seen in Table 1, carbonyl groups were less removed, which may be due to their greater stability in comparison with the other oxygenated groups. Moreover, Gao et al., [63] proposed that the reduction of GO using L-AA is carried out by two-step SN_2 nucleophilic reactions, where epoxy and hydroxyl groups could be opened by the oxygen anion of L-AA with a SN_2 nucleophilic attack. On the other hand, according to the literature, quinone (two carbonyl groups [8]) and chromene groups, which are of particular interest in the present study, have been proposed to act as redox mediators [8,49].

As known, the surface charge distribution and pH_{PZC} of carbon-based materials depend on the type and concentration of oxygen-containing groups. These results are included in Table 1 and SM (Fig. 4S). The pH_{PZC} of GO samples increased as their reduction degree was higher, from 2.3 for urGO to 6.55 and 7.25 for rGO-2 and rGO-4, respectively. The acidic surface and low pH_{PZC} of urGO is due to high concentration of carboxylic, lactonic and phenolic groups [69]. Accordingly, Boehm titrations (see Table 1) revealed that the concentration of carboxylic and phenolic groups decreased about 85% in rGO-4 sample, which was reflected in higher pH_{PZC} [70]. This is in agreement with FT-IR spectra analyses that provided additional evidence of a decrease in acidic oxygenated groups, which will be discussed later.

The surface of carbon materials may contain several functional groups whose acid-basic characteristics may or may not resemble those of individual compounds. Therefore, the presence of ionizable functional groups in the material can be given by their pKa (or pH) values [8]. Distribution of pKa values of GO samples is shown in SM (Fig. 5S). It can be observed that the most prevalent pKa value of oxygenated groups present in urGO is 2.31, which corresponds to carboxylic groups giving acidic character to the material [8]. Also, when the reduction degree of GO is higher, the most marked values are 8.25 and 10.28, suggesting the increase in basicity. It is to be noted that GO is known to be unstable at high pH OH^- can catalyze the conversion of epoxides groups to hydroxyls groups [71]. Hence, the interpretation of pKa values at high pH must be taken with care. On the other hand, the observed distributions of pKa values of ionizable oxygenated groups explain the increases of the pH_{PZC} of samples when these are further reduced (see Table 1). Similar results have been reported by Konkena and Vasudevan [72]. They concluded that GO sheets have more acidic groups, such as carboxylic groups (pKa 4.3), in comparison with rGO sheets (pKa 8.0), which was reflected in the increase of zeta potential values.

In order to evidence the removal of different functional groups through the reduction process of GO, FT-IR spectra were recorded as shown in Fig. 3. It can be observed the stretching vibration of O-H groups from 3000 to 3700 cm^{-1}. The urGO spectrum (Fig. 3A) shows bands at 1720 and 1570 cm^{-1}, corresponding to C=O stretching vibrations from carboxyl and carbonyl groups, respectively. Furthermore, stretching vibrations of C-OH

(1390 cm^{-1}), C-O from epoxy groups (1100 cm^{-1}) and ketone groups (600-630 cm^{-1}) can be observed [3,8,21,22]. As shown in rGO-2 and rGO-4 spectra (Fig. 3B and 3C), intensities of FT-IR bands associated to oxygenated groups, such as C-OH (1390 cm^{-1}) and C=O (1720 from carboxylic groups) slightly decreased, which agrees with data obtained by Boehm titrations (see Table 1). Also, the bands intensity of C-O stretching vibration (1100 cm^{-1}) dramatically decreased and the spectral signal related to ketone groups (600-630 cm^{-1}) disappeared. Furthermore, the appearance of aromatic C=C stretching vibration at 1620 cm^{-1} was also observed [73,75,76]. These results show that the bands intensities associated to oxygenated groups strongly decreased with respect to urGO, indicating the efficiency of L-AA as reducing agent. Some studies have reported that L-AA mainly remove epoxy and hydroxyl groups [73,74,77].

In addition, FT-IR spectra of urGO, rGO-2 and rGO-4 exposed to Na_2S for 1 day (GO-based materials were in contact with 2.6 mol/L of Na_2S at 25 °C and 125 rpm, and dried before analysis) showed that only rGO-based materials exhibit a band at 668 cm^{-1} associated to C-S stretching vibration (see Fig. 6S). This link can be formed due to the high nucleophilicity of reactive HS^- species and to the charge deficiency on the carbon of the carbonyl groups on rGO materials under study [16]. On the other hand, the reduction of GO by sulfur-containing compounds, such as Na_2S and Na_2SO_3, has been previously reported [78]. However, FT-IR spectra of rGO materials did not show a significant decrease of oxygenated groups, which suggest that sulfide, did not promote reduction of these functional groups in GO materials.

Besides, oxygenated groups present in GO-based materials play a fundamental role in their electrochemical properties [79]. Accordingly, the electrochemical evaluation of GO-based materials deposited on a GCE was carried out by the CV technique as shown in Fig. 4. It can be observed the reduction peak of urGO at -0.82 V (vs Ag/AgCl/KCl (saturated)) with a peak current of -0.072 mA. Ramesha and Sampath [80] reported that the reduction of GO is an irreversible electrochemically process, which began at -0.6 V (vs saturated calomel electrode (SCE)) and reaches a maximum at -0.87 V (vs SCE). Moreover, an inherent reduction peak of GO in the cathodic region around -0.7 and -0.8 V (vs Ag/AgCl) has been reported, due to possible reduction of epoxy, peroxy and aldehyde groups [81]. As it was

observed in the FT-IR spectrum of urGO, one of the identified oxygenated groups is of epoxy type at 1100 cm^{-1}. Therefore, this peak (at -0.82 V) may be related to the reduction process of these oxygenated groups present in urGO.

Furthermore, it can be seen (Fig. 4) that the intensity of the cathodic peak current (I_{PC}) varies according to the reduction degree of samples, with values of -0.031 and -0.025 mA for rGO-2 and rGO-4, respectively. It has been reported that a greater C/O atomic ratio in rGO materials is correlated with an improved electron transferring capacity, which is reflected in the current intensity [82]. In order to determine the amount of carbon and oxygen on GO-based materials, an EDS analysis was performed. Results indicated that the carbon content in urGO, rGO-2 and rGO-4 was 22.8, 37.9 and 68.9 %, respectively. Similarly, the content of oxygen in urGO, rGO-2 and rGO-4 was 77.2, 62.1 and 31.1 %, respectively. As evidenced, rGO materials contain a minor amount of oxygenated groups in their chemical structure as observed also in both FT-IR spectra and Boehm titrations, which increases the C/O ratio as the reduction degree advances. As a consequence, the removal of these oxygenated groups favors the electrons transfer along the graphitic sheets, which is reflected on the GO conductivity.

3.2. IOP Adsorption isotherms

Capacities of GO-based materials to adsorb IOP are reported in Fig. 5. The maximum adsorption capacities for IOP at an equilibrium concentration of 600 µg/L follow this order: GO> rGO-2 > rGO-4 with values of 436.37, 343.92 and 204.31 µg/g, respectively. This decrease in the IOP adsorption capacity onto rGO-based materials can be due to that the active sites in rGO are less accessible since graphene sheets tend to stack due to π-π interactions, which significantly decrease the adsorbent surface area available to IOP molecules. As mentioned in section 3.1, the removal of oxygenated groups of GO sheets increase the hydrophobicity of rGO materials forming graphene-based materials agglomerates by π-π interactions [13], which decrease the active area of materials. Furthermore, it is possible that the IOP adsorption mechanism involves hydrogen bonding interactions between ionized functional groups of GO-based materials and the hydroxyl groups present in IOP molecules [83], as shown in Fig. 7S of SM.

3.3. Chemical transformation of IOP

Chemical transformation of IOP by sulfide and the corresponding control experiments are shown in Fig. 6. The chemical reduction experiments (Na_2S + GO-based materials + IOP) exhibited a decrease in IOP concentration with removal efficiencies of 54, 58 and 66 % for incubations amended with urGO, rGO-2 and rGO-4 as RM, respectively. In contrast, control incubated in the absence of RM (Na_2S + IOP) achieved only 25% of IOP removal after 13 days. Adsorption controls (GO-based materials + IOP) showed a diminishment on the concentration of IOP < 10% in all cases. Also, a negligible removal (< 4%) occurred in stability control during the same incubation period. Moreover, the difference in IOP removal between these experiments and the adsorption controls can be attributed to the conversion of IOP to transformation byproducts.

In addition, the maximum removal rates achieved in assays amended with urGO, rGO-2 and rGO-4 were 35.84, 59.79 and 64.74 μg/L-d, respectively. Moreover, the maximum removal rate achieved in the control incubated in the absence of GO-based materials was 12.48 μg/L-d. These results indicated a 1.6 and 1.8-fold increase in the maximum removal rate of IOP in the presence of rGO-2 and rGO-4, respectively, with respect to urGO. Moreover, the maximum removal rate of IOP increased 2.8, 4.8 and 5.2-fold in the presence of urGO, rGO-2 and rGO-4, respectively, with respect to the control lacking GO-based materials. These results demonstrate that GO-based materials promoted a faster removal of IOP. In the following section, it will be confirmed that GO-based materials serve as effective redox mediators achieving a greater extent of IOP transformation.

3.4. Transformation pathway of IOP

Samples derived from reduction experiments of IOP in the presence of rGO-4 as redox mediator were analyzed by HPLC-MS in order to propose the transformation pathway of IOP. Based on HPLC-MS analysis, six transformation products (TPs, see Fig. 8S in SM) were identified and the suggested chemical transformation pathway of IOP is shown in Fig 7.

The structure of TP 788.70 (elemental composition $C_{18}H_{22}I_3N_3O_8$) was proposed by Eversloh et al., [84], which indicates that this intermediate could be obtained by a loss of

two hydrogen atoms at either side chain A or B. The structure of this TP is exemplified in Fig. 7 as the loss of hydrogen atoms taking place in side chain A. The structure of TP 774 (elemental composition $C_{18}H_{24}I_3N_3O_7$) implies the loss of a molecule of H_2O at side chain B as reported by Pérez et al., [85] and Gros et al., [86]. Also, the structure of TP 722.5 (elemental composition $C_{15}H_{20}I_3N_3O_6$) suggests the loss of a molecule of H_2O, demethylation and decarboxylation in side chain B and N-demethylation in side chain A. Similar mechanisms and structure have also been proposed by Gros et al. [86].

The cleavage of the amide bond in side chain B and removal of one iodine atom (HI) of TP 788.7 results in the formation of TP 574 (elemental composition $C_{15}H_{15}I_2N_2O_6$) as shown in Fig. 7. This structure is similar to that reported by Gros et al. [86]. Moreover, the structure of TP 634.60 (elemental composition $C_{17}H_{23}I_2N_3O_7$) was proposed according to previous studies [86], which indicate that this intermediate is formed by the loss of one iodine atom (HI) and N-demethylation in side chain A of TP 774. Finally, the structure of TP 314.8 (elemental composition $C_{10}H_4INO_3^+$) suggests the removal of side chain A and one iodine atom (HI) of TP 574. The removal of HI yielded a five membered ring structure in side chain C. Similar transformation pathways were reported by Schulz et al., [87] under aerobic conditions.

The results obtained from batch experiments performed without RM (IOP + Na_2S control) revealed that the main TPs produced were 646.9, 768.7 and 788.8 (See SM, Fig. 7S). According to these results, it can be concluded that the presence of GO-based materials as RM promoted a higher extent of IOP transformation (involving dehalogenation, dehydration, demethylation and decarboxylation reactions), as compared to control incubations performed in the absence of GO-based materials, which was evidenced by the formation of TPs with low m/z, such as TP 634.6, TP 574 and TP 314.8. The reductive transformation of IOP and distinct capacities of GO-based materials to act as redox mediator can be explained by their surface chemistry as discussed in the next section.

3.5. Mechanisms of IOP transformation mediated by GO-based materials

The proposed transformation mechanism implies that GO-based materials promoted dehalogenation, dehydration, demethylation and decarboxylation reactions in IOP molecule. Previous studies have reported that carbonaceous materials can mediate reductive reactions of organic compounds by enhancing the electron transfer involved in the reactions [9,29]. In this sense, the reduction of recalcitrant pollutants, such as nitroaromatics, azo dyes and polyhalogenated compounds, promoted by GO as redox mediator has been reported [5,30,31,33]. In addition, it has been reported that the zigzag edges of reduced GO can accelerate the reduction reaction of reactants [6]. In consequence, the increased IOP transformation observed in the presence of rGO-materials can be explained by enhanced electron transfer and possibly by activation of IOP molecules. As mentioned above, the basal plane of GO sheets has very high electric conductivity that depends on the presence of epoxy and hydroxyl groups and is generally proportional to the C/O ratio. As mentioned in section 3.1, as the C/O ratio increased in rGO materials the electron transfer on basal plane improved, which was reflected in an increased reduction of IOP. Additionally, as revealed by Boehm titration results (see Table 1) rGO materials have a higher percentage of quinone groups (referring to two carbonyl groups), which could contribute to the reduction of IOP since these functional groups serve as redox mediating moieties [8,49] and improved the electric conductivity, i.e. electron transfer of the materials, making best mediators for electron transfer [5].

On the other hand, it has been reported that carbonaceous materials with basic properties exhibit a better performance to transfer electrons through quinone groups or delocalized π-electrons [88]. As discussed in section 3.1, the basic properties of GO-based materials increased with the reduction degree, which was reflected in a higher pH_{PZC} (see Table 1). This also explains why the reductive transformation of IOP increased when the materials used as redox mediator had a greater reduction degree.

Additionally, it has also been stated that the carbon atoms at the zigzag edges of graphene sheets have high chemical reactivity due to the non-bonding π-electrons localized at the zigzag site, and hence, are able to interact strongly with H, OH or halogen groups [89]. The IOP molecule has hydroxyl and halogenated (iodated) groups in its chemical structure,

which might well interact with the carbon atoms at zigzag edges, favoring the reduction of this pollutant and improving the mediation effect of rGO-based materials as observed in Fig. 6.

4. Summary

The results demonstrated the importance of the chemical and physical properties of GO-based materials to serve as electron shuttle in the chemical transformation of IOP. Moreover, the characterization of rGO-based materials indicated a decrease on oxygen content of 19.1 % and 64.4 % for rGO-2 and rGO-4, respectively, which was related to the reduction and transformation degree of IOP. Chemical reduction experiments demonstrated, for the first time, that GO-based materials can act as redox mediators for the abiotic transformation of IOP with sulfide as electron donor, involving dehalogenation, dehydration, demethylation and decarboxylation reactions. The catalytic activity of materials decreases as follows: rGO-4> rGO-2> urGO, due to the partially removal of oxygenated groups, which enhanced the electronic conductivity of the basal plane of the GO sheets towards the model pollutant. Moreover, the presence of oxygenated functional groups at the edge of GO-based materials sheets, such as quinone groups, can also act as electron shuttles that are capable of electron transfer, which was reflected in a better catalytic input in IOP transformation. This is supported by the stability and high concentration of quinone groups after chemical reduction of GO. Moreover, the reduction of IOP could be enhanced by strong interaction between its hydroxyl and halogenated (iodides) and the carbon atoms on zigzag edges of graphene sheets. Chemical transformation products with a simpler structure than IOP were identified by HPLC-MS, which is the first step towards their mineralization possibly by aerobic processes in a second stage. Also, the chemical transformation pathway of IOP was proposed. Finally, the properties of GO-based materials, such as zeta potential, ORP, pH_{PZC} and conductivity, played an important role in the electron transfer for reductive transformation of IOP.

Acknowledgements

The authors greatly acknowledge the financial support from the Council of Science and Technology of Mexico (Grants SEP-CB-2014-237118 and SEP-CONACYT 155656) and from the Marcos Moshinsky Foundation. In addition, the authors also appreciate the help provided by Laboratorio Nacional de Biotecnología Agrícola, Médica y Ambiental (LANBAMA, IPICYT) and Laboratorio de Investigaciones en Nanociencias y Nanotecnología (LINAN, IPICYT), as well as the technical support of A. Colunga-Álvarez, D. Partida-Gutiérrez, G. Vidriales-Escobar, J.P. Rodas-Ortiz, B. Rivera-Escoto, Mireya Martínez-Pérez, G. Labrada-Delgado and Ma. del C. Rocha-Medina.

References

[1] Geim AK. Graphene: Status and prospects. Science 2009;324:1530–4. doi:10.1126/science.1158877.

[2] Stankovich S, Dikin DA, Dommett GHB, Kohlhaas KM, Zimney EJ, Stach EA, et al. Graphene-based composite materials. Nature 2006;442:282–6. doi:10.1038/nature04969.

[3] Geim AK, Novoselov KS. The rise of graphene. Nat Mater 2007;6:183–91. doi:10.1038/nmat1849.

[4] Enoki T, Kobayashi Y, Fukui K. Electronic structures of graphene edges and nanographene. Int Rev Phys Chem - INT REV PHYS CHEM 2007;26:609–45. doi:10.1080/01442350701611991.

[5] Fu H, Zhu D. Graphene oxide-facilitated reduction of nitrobenzene in sulfide-containing aqueous solutions. Environ Sci Technol 2013;47:4204–10. doi:10.1021/es304872k.

[6] Gao Y, Ma D, Wang C, Guan J, Bao X. Reduced graphene oxide as a catalyst for hydrogenation of nitrobenzene at room temperature. Chem Commun 2011;47:2432–4. doi:10.1039/C0CC04420B.

[7] Agnoli S, Granozzi G. Second generation graphene: Opportunities and challenges for surface science. Surf Sci 2013;609:1–5. doi:10.1016/j.susc.2012.11.016.

559 [8] Leon y Leon CA, Radovic LR. Interfacial chemistry and electrochemistry of carbon
560 surfaces. Chem. Phys. Carbon, vol. 2, New York: Peter A. Thrower Marcel Delcker;
561 1994, p. 213–311.
562 [9] van der Zee FP, Bisschops IAE, Lettinga G, Field JA. Activated carbon as an electron
563 acceptor and redox mediator during the anaerobic biotransformation of azo dyes.
564 Environ Sci Technol 2003;37:402–8. doi:10.1021/es025885o.
565 [10] Cervantes FJ, van der Velde S, Lettinga G, Field JA. Quinones as terminal electron
566 acceptors for anaerobic microbial oxidation of phenolic compounds. Biodegradation
567 2000;11:313–21.
568 [11] Pereira RA, Pereira MFR, Alves MM, Pereira L. Carbon based materials as novel
569 redox mediators for dye wastewater biodegradation. Appl Catal B Environ
570 2014;144:713–20. doi:10.1016/j.apcatb.2013.07.009.
571 [12] van der Zee FP, Cervantes FJ. Impact and application of electron shuttles on the redox
572 (bio)transformation of contaminants: A review. Biotechnol Adv 2009;27:256–77.
573 doi:10.1016/j.biotechadv.2009.01.004.
574 [13] Stankovich S, Dikin DA, Piner DR, Kohlhaas KA, Kleinhammes A, Jia Y, et al.
575 Synthesis of graphene-based nanosheets via chemical reduction of exfoliated graphite
576 oxide. Carbon. 45 (2007) 1558–1565. doi:10.1016/j.carbon.2007.02.034.
577 [14] Dreyer DR, Park S, Bielawski CW, Ruoff RS. The chemistry of graphene oxide.
578 Chem Soc Rev 2009;39:228–40. doi:10.1039/B917103G.
579 [15] Rios-Del Toro E, Celis LB, Cervantes FJ, Rangel-Mendez JR. Enhanced microbial
580 decolorization of methyl red with oxidized carbon fiber as redox mediator. J Hazard
581 Mater 2013;260:967–74. doi:10.1016/j.jhazmat.2013.06.056.
582 [16] Amezquita-Garcia HJ, Razo-Flores E, Cervantes FJ, Rangel-Mendez JR. Activated
583 carbon fibers as redox mediators for the increased reduction of nitroaromatics. Carbon
584 2013;55:276–84. doi:10.1016/j.carbon.2012.12.062.
585 [17] Oh SY, Chiu PC. Graphite- and soot-mediated reduction of 2,4-dinitrotoluene and
586 hexahydro-1,3,5-trinitro-1,3,5-triazine. Environ. Sci. Technol. 2009;43:6983–88.
587 doi:10.1021/es901433m.
588 [18] Gong W, Liu X, Tao L, Xue W, Fu W, Cheng D. Reduction of nitrobenzene with
589 sulfides catalyzed by the black carbons from crop-residue ashes. Environ. Sci. Pollut.

590 Res 2014; 21:6162–69. doi:10.1007/s11356-014-2533-4.
591 [19] Xu W, Pignatello JJ, Mitch WA. Reduction of nitroaromatics sorbed to black carbon
592 by direct reaction with sorbed sulfides. Environ. Sci. Technol 2015;49:3419–26.
593 doi:10.1021/es5045198.
594 [20] Yu X, Gong W, Liu X, Shi L, Han X, Bao H. The use of carbon black to catalyze the
595 reduction of nitrobenzenes by sulfides. J. Hazard. Mater 2011:198:340–6.
596 doi:10.1016/j.jhazmat.2011.10.052.
597 [21] Oh SY, Son JG, Chiu PC. Black carbon-mediated reductive transformation of nitro
598 compounds by hydrogen sulfide. Environ. Earth Sci 2014;73:1813–22.
599 doi:10.1007/s12665-014-3535-8.
600 [22] Millerick K, Drew SR, Finneran KT. Electron shuttle-mediated biotransformation of
601 hexahydro-1,3,5-trinitro-1,3,5-triazine adsorbed to granular activated carbon.
602 Environ. Sci. Technol 2013;47:8743–50. doi:10.1021/es401641s.
603 [23] Kemper JM, Ammar E, Mitch WA. Abiotic degradation of hexahydro-1,3,5-trinitro-
604 1,3,5-triazine in the presence of hydrogen sulfide and black carbon. Environ. Sci.
605 Technol 2008;42:2118–23. doi:10.1021/es702402a.
606 [24] Xu W, Pignatello JJ, Mitch WA. Role of black carbon electrical conductivity in
607 mediating hexahydro-1,3,5-trinitro-1,3,5-triazine (RDX) transformation on carbon
608 surfaces by sulfides. Environ. Sci. Technol 2013;47:7129–36.
609 doi:10.1021/es4012367.
610 [25] Xu W, Dana KE, Mitch WA. Black carbon-mediated destruction of nitroglycerin and
611 RDX by hydrogen sulfide. Environ. Sci. Technol 2010;44:6409–15.
612 doi:10.1021/es101307n.
613 [26] Oh SY, Son JG, Chiu PC. Biochar-mediated reductive transformation of nitro
614 herbicides and explosives. Environ. Toxicol. Chem 32 2013;32:501–8.
615 doi:10.1002/etc.2087.
616 [27] Oh SY, Son JG, Lim OT, Chiu PC. The role of black carbon as a catalyst for
617 environmental redox transformation. Environ. Geochem. Health 2014;34:105–13.
618 doi:10.1007/s10653-011-9416-0.
619 [28] Chen W, Zhu D, Zheng S, Chen W. Catalytic effects of functionalized carbon
620 nanotubes on dehydrochlorination of 1,1,2,2-tetrachloroethane. Environ. Sci. Technol

621 2014;48:3856–63. doi:10.1021/es405683d.
622 [29] Larsen JW, Freund M, Kim KY, Sidovar M, Stuart JL. Mechanism of the carbon
623 catalyzed reduction of nitrobenzene by hydrazine. Carbon 2000;38:655–61.
624 doi:10.1016/S0008-6223(99)00155-4.
625 [30] Colunga A, Rangel-Mendez JR, Celis LB, Cervantes FJ. Graphene oxide as electron
626 shuttle for increased redox conversion of contaminants under methanogenic and
627 sulfate-reducing conditions. Bioresour Technol 2015;175:309–14.
628 doi:10.1016/j.biortech.2014.10.101.
629 [31] Lu H, Zhang H, Wang J, Zhou J, Zhou Y. A novel quinone/reduced graphene oxide
630 composite as a solid-phase redox mediator for chemical and biological acid yellow 36
631 reduction. RSC Adv 2014;4:47297–303. doi:10.1039/C4RA08817D.
632 [32] Wang J, Wang D, Liu G, Jin R, Lu H. Enhanced nitrobenzene biotransformation by
633 graphene-anaerobic sludge composite. J. Chem. Technol. Biotechnol 2014;89: 750–5.
634 doi:10.1002/jctb.4182.
635 [33] Fu H, Guo Y, Chen W, Gu C, Zhu D. Reductive dechlorination of hexachloroethane
636 by sulfide in aqueous solutions mediated by graphene oxide and carbon nanotubes.
637 Carbon 2014;72:74–81. doi:10.1016/j.carbon.2014.01.053.
638 [34] Hennebel T, De Corte S, Vanhaecke L, Vanherck K, Forrez I, De Gusseme B, et al.
639 Removal of diatrizoate with catalytically active membranes incorporating microbially
640 produced palladium nanoparticles. Water Res 2010;44:1498–506.
641 [35] Busetti F, Linge KL, Rodriguez C, Heitz A. Occurrence of iodinated X-ray contrast
642 media in indirect potable reuse systems. J Environ Sci Health Part A Tox Hazard
643 Subst Environ Eng 2010;45:542–8. doi:10.1080/10934521003595100.
644 [36] Putschew A, Wischnack S, Jekel M. Occurrence of triiodinated X-ray contrast agents
645 in the aquatic environment. Sci Total Environ 2000;255:129–34. doi:10.1016/S0048-
646 9697(00)00461-7.
647 [37] Bottinor W, Polkampally P, Jovin I. Adverse reactions to iodinated contrast media.
648 Int J Angiol Off Publ Int Coll Angiol Inc 2013;22:149–54. doi:10.1055/s-0033-
649 1348885.

650 [38] Carballa M, Omil F, Lema JM, Llompart M, García-Jares C, Rodríguez I, et al.
651 Behavior of pharmaceuticals, cosmetics and hormones in a sewage treatment plant.
652 Water Res 2004;38:2918–26. doi:10.1016/j.watres.2004.03.029.
653 [39] Onesios KM, Yu JT, Bouwer EJ. Biodegradation and removal of pharmaceuticals and
654 personal care products in treatment systems: a review. Biodegradation 2009;20:441–
655 66. doi:10.1007/s10532-008-9237-8.
656 [40] Ternes TA, Hirsch R. Occurrence and behavior of X-ray contrast media in sewage
657 facilities and the aquatic environment. Environ Sci Technol 2000;34:2741–8.
658 doi:10.1021/es991118m.
659 [41] Haiß A, Kümmerer K. Biodegradability of the X-ray contrast compound diatrizoic
660 acid, identification of aerobic degradation products and effects against sewage sludge
661 micro-organisms. Chemosphere 2006;62:294–302.
662 doi:10.1016/j.chemosphere.2005.05.007.
663 [42] Boehm HP. Some aspects of the surface chemistry of carbon blacks and other carbons.
664 Carbon 1994;32:759–69. doi:10.1016/0008-6223(94)90031-0.
665 [43] Bandosz TJ, Jagiello J, Contescu C, Schwarz JA. Characterization of the surfaces of
666 activated carbons in terms of their acidity constant distributions. Carbon
667 1993;31:1193–202. doi:10.1016/0008-6223(93)90072-I.
668 [44] Jagiello J. Stable numerical solution of the adsorption integral equation using splines.
669 Langmuir 1994;10:2778–85. doi:10.1021/la00020a045.
670 [45] Li Y, Du Q, Liu T, Peng X, Wang J, Sun J, et al. Comparative study of methylene
671 blue dye adsorption onto activated carbon, graphene oxide, and carbon nanotubes.
672 Chem Eng Res Des 2013;91:361–8. doi:10.1016/j.cherd.2012.07.007.
673 [46] Krishnamoorthy K, Veerapandian M, Yun K, Kim S-J. The chemical and structural
674 analysis of graphene oxide with different degrees of oxidation. Carbon 2013;53:38–
675 49. doi:10.1016/j.carbon.2012.10.013.
676 [47] Jung I, Dikin DA, Piner RD, Ruoff RS. Tunable electrical conductivity of individual
677 graphene oxide sheets reduced at “low” temperatures. Nano Lett 2008;8:4283–7.
678 doi:10.1021/nl8019938.
679 [48] Pansu M, Gautheyrou J. Redox potential. Handb. Soils Anal. 1st ed., Germany:
680 Springer-Verlag Berlin Heidelberg; 2006, p. 581–91.

[49] Montes-Morán MA, Suárez D, Menéndez JA, Fuente E. On the nature of basic sites on carbon surfaces: an overview. Carbon 2004;42:1219–25. doi:10.1016/j.carbon.2004.01.023.

[50] Menéndez JA, Phillips J, Xia B, Radovic LR. On the modification and characterization of chemical surface properties of activated carbon: In the search of carbons with stable basic properties. Langmuir 1996;12:4404–10. doi:10.1021/la9602022.

[51] Moreno-Castilla C, Rivera-Utrilla J, Joly JP, López-Ramón MV, Ferro-García MA, Carrasco-Marín F. Thermal regeneration of an activated carbon exhausted with different substituted phenols. Carbon 1995;33:1417–23. doi:10.1016/0008-6223(95)00090-Z.

[52] Noh CH, Jung JE, Kim JY, Sakong DS, Choi KS. A Study on the morphology and electro-optic properties of liquid crystal-polymer composite films. Mol Cryst Liq Cryst Sci Technol Sect Mol Cryst Liq Cryst 1993;237:299–309. doi:10.1080/10587259308030144.

[53] Deng Y, Gu A, Fang Z. The effect of morphology on the optical properties of transparent epoxy/montmorillonite composites. Polym Int 2004;53:85–91. doi:10.1002/pi.1410.

[54] Nair RR, Blake P, Grigorenko AN, Novoselov KS, Booth TJ, Stauber T, et al. Fine structure constant defines visual transparency of graphene. Science 2008;320:1308–1308. doi:10.1126/science.1156965.

[55] Niyogi S, Bekyarova E, Itkis ME, McWilliams JL, Hamon MA, Haddon RC. Solution properties of graphite and graphene. J Am Chem Soc 2006;128:7720–1. doi:10.1021/ja060680r.

[56] Wang G, Yang J, Park J, Gou X, Wang B, Liu H, et al. Facile synthesis and characterization of graphene nanosheets. J Phys Chem C 2008;112:8192–5. doi:10.1021/jp710931h.

[57] Venugopal G, Jung M-H, Suemitsu M, Kim S-J. Fabrication of nanoscale three-dimensional graphite stacked junctions by focused-ion-beam and observation of anomalous transport characteristics. Carbon 2011;49:2766–72. doi:10.1016/j.carbon.2011.03.003.

712 [58] Ferrari AC, Robertson J. Interpretation of Raman spectra of disordered and
713 amorphous carbon. Phys Rev B 2000;61:14095–107.
714 doi:10.1103/PhysRevB.61.14095.
715 [59] Tuinstra F, Koenig JL. Raman spectrum of graphite. J Chem Phys 1970;53:1126–30.
716 doi:10.1063/1.1674108.
717 [60] Chen W, Yan L, Bangal PR. Preparation of graphene by the rapid and mild thermal
718 reduction of graphene oxide induced by microwaves. Carbon 2010;48:1146–52.
719 doi:10.1016/j.carbon.2009.11.037.
720 [61] Paredes JI, Villar-Rodil S, Solís-Fernández P, Martínez-Alonso A, Tascón JMD.
721 Atomic force and scanning tunneling microscopy imaging of graphene nanosheets
722 derived from graphite oxide. Langmuir 2009;25:5957–68. doi:10.1021/la804216z.
723 [62] Solís-Fernández P, Rozada R, Paredes JI, Villar-Rodil S, Fernández-Merino MJ,
724 Guardia L, et al. Chemical and microscopic analysis of graphene prepared by
725 different reduction degrees of graphene oxide. J Alloys Compd 2012;536,
726 Supplement 1:S532–7. doi:10.1016/j.jallcom.2012.01.102.
727 [63] Gao J, Liu F, Liu Y, Ma N, Wang Z, Zhang X. Environment-friendly method to
728 produce graphene that employs vitamin C and amino acid. Chem Mater
729 2010;22:2213–8. doi:10.1021/cm902635j.
730 [64] Knight DS, White WB. Characterization of diamond films by Raman spectroscopy. J
731 Mater Res 1989;4:385–93. doi:10.1557/JMR.1989.0385.
732 [65] Cançado LG, Takai K, Enoki T, Endo M, Kim YA, Mizusaki H, et al. General
733 equation for the determination of the crystallite size La of nanographite by Raman
734 spectroscopy. Appl Phys Lett 2006;88:163106. doi:10.1063/1.2196057.
735 [66] Pei S, Cheng H-M. The reduction of graphene oxide. Carbon 2012;50:3210–28.
736 doi:10.1016/j.carbon.2011.11.010.
737 [67] Kim MC, Hwang GS, Ruoff RS. Epoxide reduction with hydrazine on graphene: a
738 first principles study. J Chem Phys 2009;131:064704. doi:10.1063/1.3197007.
739 [68] Gao X, Jang J, Nagase S. Hydrazine and thermal reduction of graphene oxide:
740 reaction mechanisms, product structures, and reaction design. J Phys Chem C
741 2010;114:832–42. doi:10.1021/jp909284g.

[69] Boehm HP. Surface oxides on carbon and their analysis: a critical assessment. Carbon 2002;40:145–9. doi:10.1016/S0008-6223(01)00165-8.

[70] Briceño NO, Guzmán MY, Díaz J de J. Surface Groups on carbonaceous materials. characterization by different techniques. Rev Colomb Quím 2007;36:121–30.

[71] Taniguchi T, Kurihara S, Tateishi H, Hatakeyama K, Koinuma M, Yokoi H, et al. pH-driven, reversible epoxy ring opening/closing in graphene oxide. Carbon 2015;84 560–6. doi:10.1016/j.carbon.2014.12.054.

[72] Konkena B, Vasudevan S. Understanding aqueous dispersibility of graphene oxide and reduced graphene oxide through pKa measurements. J Phys Chem Lett 2012;3:867–72. doi:10.1021/jz300236w.

[73] Fernández-Merino MJ, Guardia L, Paredes JI, Villar-Rodil S, Solís-Fernández P, Martínez-Alonso A, et al. Vitamin C is an ideal substitute for hydrazine in the reduction of graphene oxide suspensions. J Phys Chem C 2010;114:6426–32. doi:10.1021/jp100603h.

[74] Zhang J, Yang H, Shen G, Cheng P, Zhang J, Guo S. Reduction of graphene oxide via L-ascorbic acid. Chem Commun 2010;46:1112–4. doi:10.1039/B917705A.

[75] Guo HL, Wang XF, Qian QY, Wang FB, Xia XH. A Green approach to the synthesis of graphene nanosheets. ACS Nano 2009;3:2653–9. doi:10.1021/nn900227d.

[76] Chen W, Yan L. Preparation of graphene by a low-temperature thermal reduction at atmosphere pressure. Nanoscale 2010;2:559–63. doi:10.1039/B9NR00191C.

[77] Castro-Beltrán A, Sepúlveda-Guzmán S, De la Cruz-Hernández W, Cruz-Silva R. Obtención de grafeno mediante la reducción química del óxido de grafito. Ingenierías 2011;14:34–43.

[78] Chen W, Yan L, Bangal PR. Chemical reduction of graphene oxide to graphene by sulfur-containing compounds. J Phys Chem C 2010;114:19885–90. doi:10.1021/jp107131v.

[79] Pumera M. Electrochemistry of graphene, graphene oxide and other graphenoids: Review. Electrochem Commun 2013;36:14–8. doi:10.1016/j.elecom.2013.08.028.

[80] Ramesha GK, Sampath S. Electrochemical reduction of oriented graphene oxide films: An in situ raman spectroelectrochemical study. J Phys Chem C 2009;113:7985–9.

773 doi:10.1021/jp811377n.
774 [81] Zhou M, Wang Y, Zhai Y, Zhai J, Ren W, Wang F, et al. Controlled synthesis of
775 large-area and patterned electrochemically reduced graphene oxide films. Chem – Eur
776 J 2009;15:6116–20. doi:10.1002/chem.200900596.
777 [82] Ambrosi A, Chua CK, Khezri B, Sofer Z, Webster RD, Pumera M. Chemically
778 reduced graphene contains inherent metallic impurities present in parent natural and
779 synthetic graphite. Proc Natl Acad Sci U S A 2012;109:12899–904.
780 doi:10.1073/pnas.1205388109.
781 [83] Kim H, Hwang YS, Sharma VK. Adsorption of antibiotics and iopromide onto single-
782 walled and multi-walled carbon nanotubes. Chem Eng J 2014;255:23–7.
783 doi:10.1016/j.cej.2014.06.035.
784 [84] Lütke Eversloh C, Henning N, Schulz M, Ternes TA. Electrochemical treatment of
785 iopromide under conditions of reverse osmosis concentrates – Elucidation of the
786 degradation pathway. Water Res 2014;48:237–46. doi:10.1016/j.watres.2013.09.035.
787 [85] Pérez S, Eichhorn P, Celiz MD, Aga DS. Structural characterization of metabolites of
788 the X-ray contrast agent iopromide in activated sludge using ion trap mass
789 spectrometry. Anal Chem 2006;78:1866–74. doi:10.1021/ac0518809.
790 [86] Gros M, Cruz-Morato C, Marco-Urrea E, Longrée P, Singer H, Sarrà M, et al.
791 Biodegradation of the X-ray contrast agent iopromide and the fluoroquinolone
792 antibiotic ofloxacin by the white rot fungus Trametes versicolor in hospital
793 wastewaters and identification of degradation products. Water Res 2014;60:228–41.
794 doi:10.1016/j.watres.2014.04.042.
795 [87] Schulz M, Löffler D, Wagner M, Ternes TA. Transformation of the X-ray contrast
796 medium iopromide in soil and biological wastewater treatment. Environ Sci Technol
797 2008;42:7207–17. doi:10.1021/es800789r.
798 [88] Pereira L, Pereira R, Pereira MFR, van der Zee FP, Cervantes FJ, Alves MM. Thermal
799 modification of activated carbon surface chemistry improves its capacity as redox
800 mediator for azo dye reduction. J Hazard Mater 2010;183:931–9.
801 doi:10.1016/j.jhazmat.2010.08.005.
802
803

804 [89] Jiang D, Sumpter BG, Dai S. The unique chemical reactivity of a graphene
805 nanoribbon's zigzag edge. J Chem Phys 2007;126:134701. doi:10.1063/1.2715558.
806

807

ACCEPTED MANUSCRIPT

ACCEPTED MANUSCRIPT

Tables

Table 1. Surface chemical properties of GO-based materials with different reduction degrees

Samples	Acid-base functional groups, (meq/L)					Point of Zero Charge (pH_{PZC})
	Carboxylic	Lactonic	Phenolic	Carbonyl	Total	
GO	1.30	1.26	0.59	1.23	4.39	2.30
rGO-2	0.34	0.84	0.21	1.29	3.55	6.55
rGO-4	0.20	0.21	0.14	1.10	1.65	7.25

ACCEPTED MANUSCRIPT

Figures

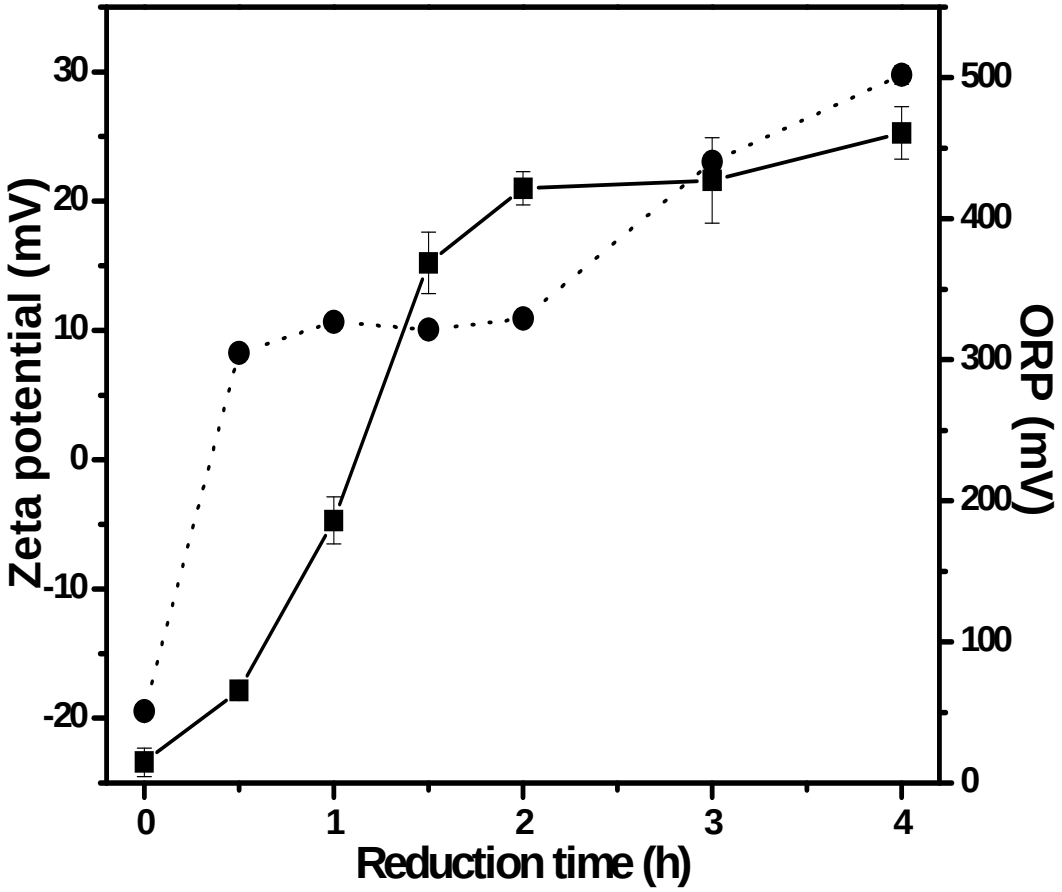

Fig. 1- Zeta potential (square symbols) and oxidation reduction potential (ORP, circle symbols) of GO-based materials with different reduction degrees at pH 7

ACCEPTED

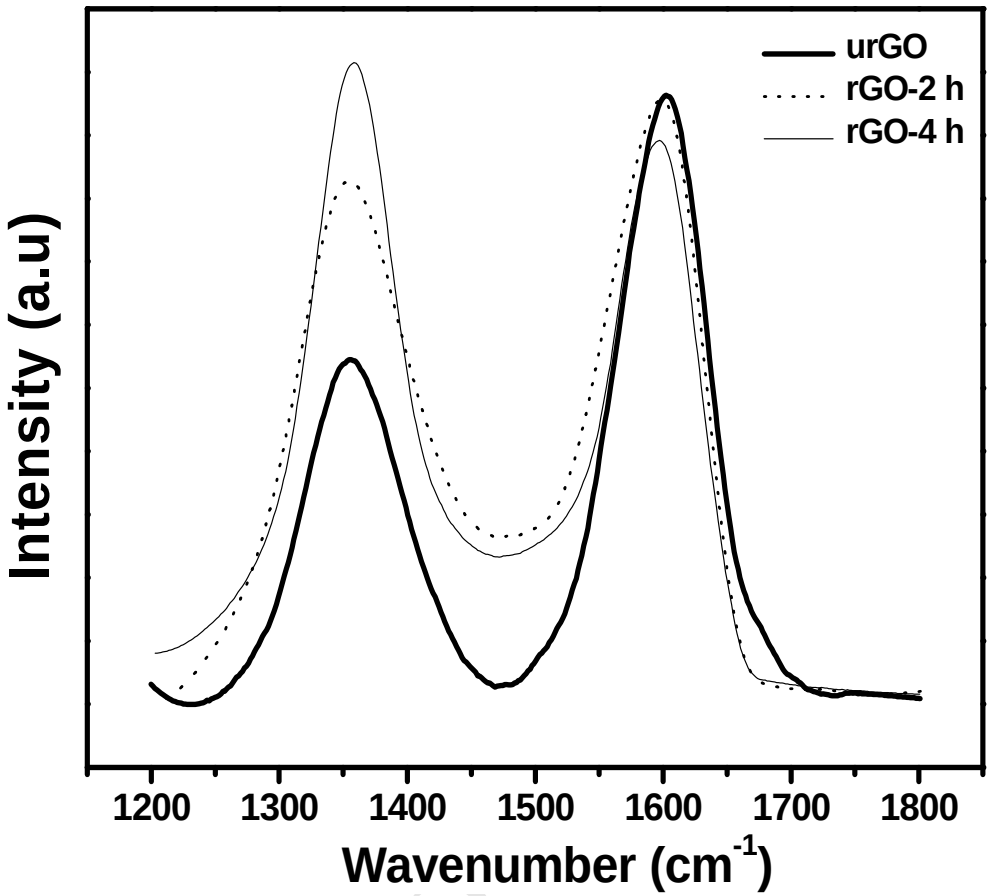

Fig. 2- Raman spectra of GO-based materials.

ACCEPTED

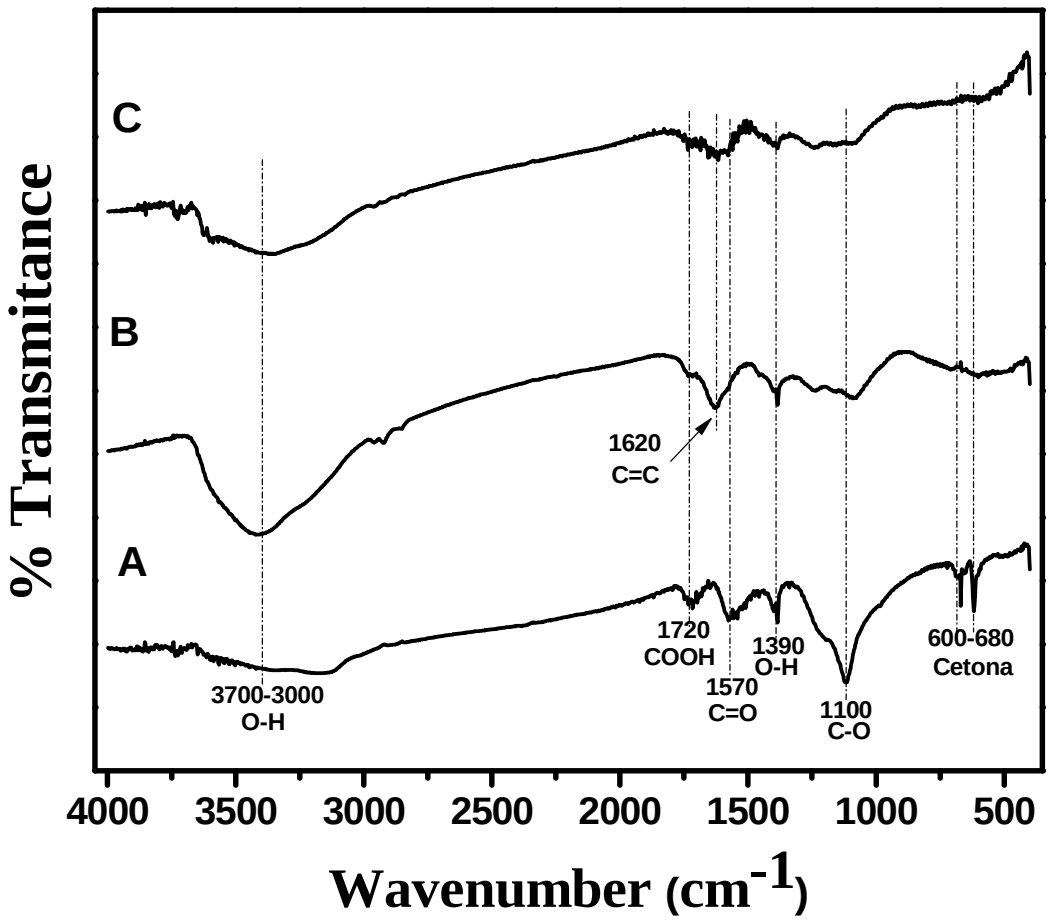

Fig. 3- FT-IR spectra of GO-based materials: (A) urGO, (B) rGO-2 h and (C) rGO-4 h.

ACCEPTED

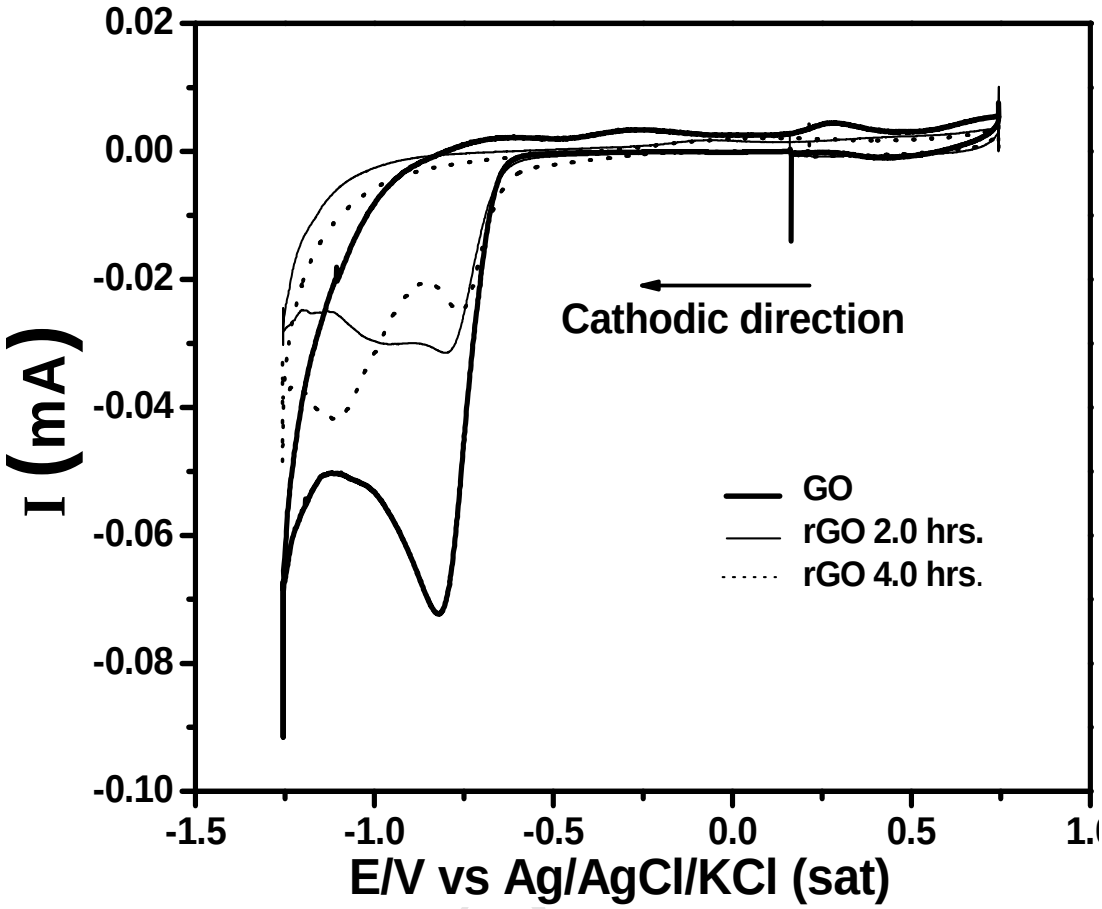

Fig. 4- Cyclic voltammetry of GO-based materials deposited on GCE electrode and immersed in a phosphate buffer (pH 7.6). The potential scan started at 0.16 V (vs Ag/AgCl/KCl (sat)) in cathodic direction to a scan rate of 20 mV/s.

ACCEPTED

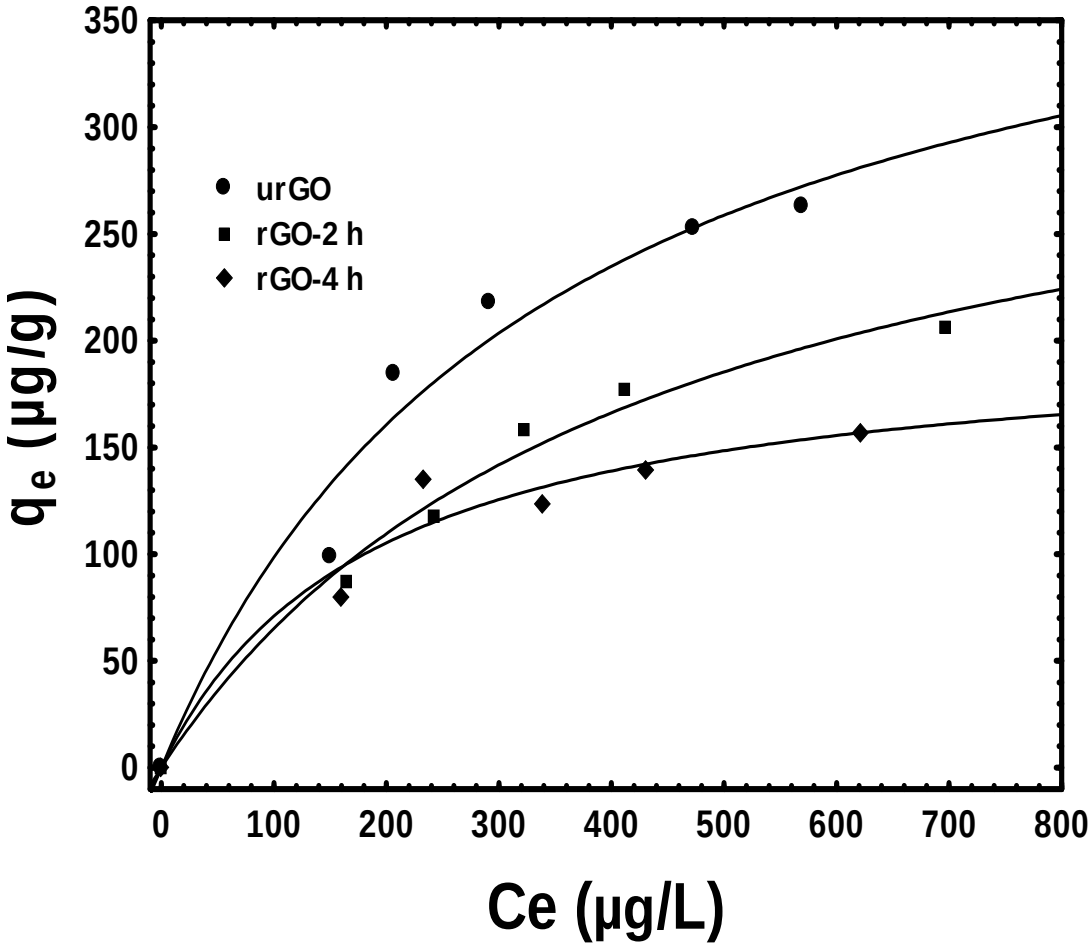

Fig. 5- Adsorption isotherms of IOP on GO-based materials with different reduction degrees at pH 7.6 and 25 °C.

ACCEPTED

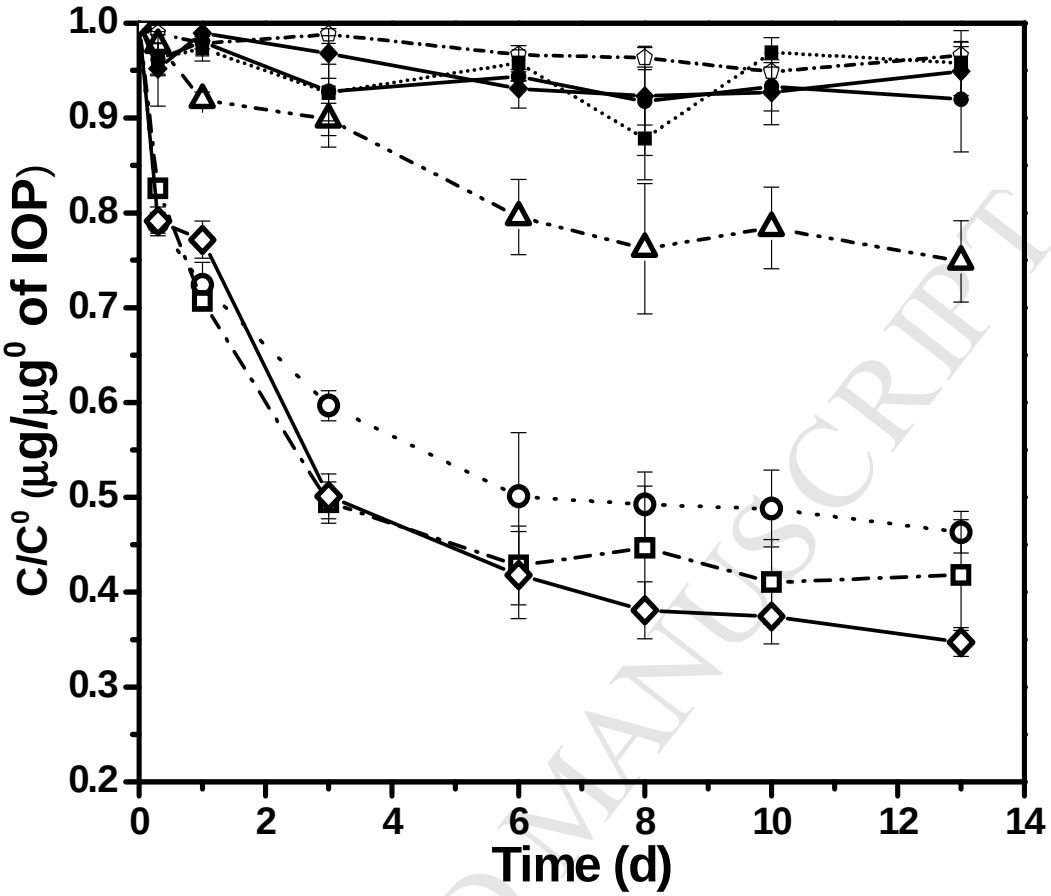

Fig. 6- GO-based materials catalysis of IOP reduction by sulfide. IOP stability control (pentagon symbol), direct chemical reduction control (triangle symbol, IOP + Na_2S), adsorption controls (full symbols, IOP + GO-based materials) and reduction experiments (open symbols, IOP + Na_2S + GO-based materials) of urGO (circles), rGO-2 h (squares) and rGO-4 h (Diamonds).

ACCEPTED MANUSCRIPT

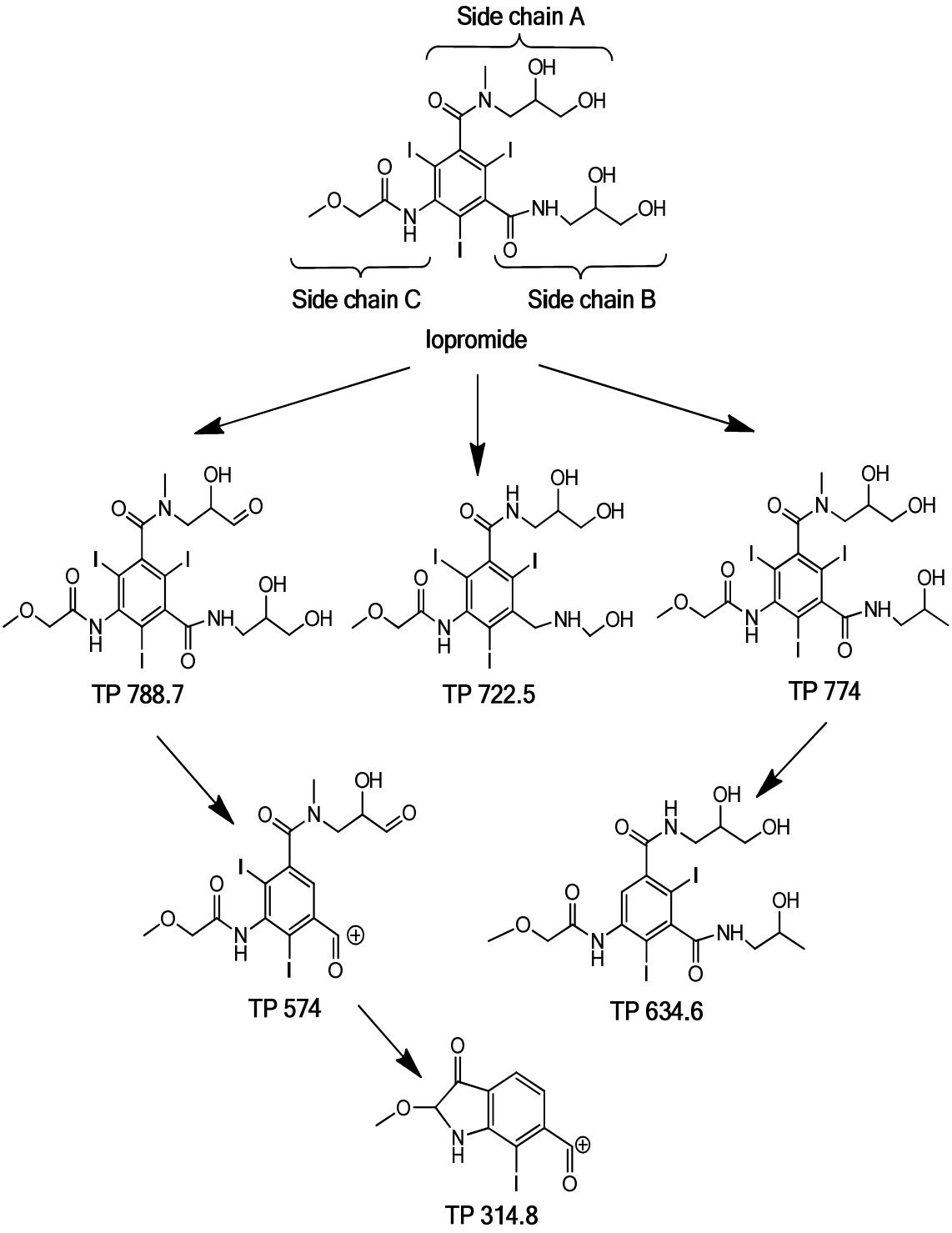

Fig. 7- Proposed chemical transformation pathway of IOP and final products by rGO-4 h as redox mediator.